THE JOURNAL OF PHYSICAL CHEMISTRY C

Article

Cite This: J. Phys. Chem. C 2018, 122, 20571−20580

pubs.acs.org/JPCC

Dynamics of Formation of a Vapor Nanobubble Around a Heated Nanoparticle

Shantanu Maheshwari,[†] Martin van der Hoef,[†] Andrea Prosperetti,[‡,†] and Detlef Lohse*[,†,§]

[†]Physics of Fluids, Max Planck Center Twente for Complex Fluid Dynamics, Mesa+ Institute, and J. M. Burgers Centre for Fluid Dynamics, Department of Science and Technology, University of Twente, P.O. Box 217, 7500 AE Enschede, The Netherlands

[‡]Department of Mechanical Engineering, University of Houston, 4726 Calhoun Road, Houston, Texas 77204-4006, United States

[§]Max Planck Institute for Dynamics and Self-Organization, 37077 Göttingen, Germany

Supporting Information

ABSTRACT: We study the formation of a nanobubble around a heated nanoparticle in a bulk liquid by using molecular dynamics simulations. The nanoparticle is kept at a temperature above the critical temperature of the surrounding liquid, leading to the formation of a vapor nanobubble attached to it. First, we study the role of both the temperature of the bulk liquid far away from the nanoparticle surface and the temperature of the nanoparticle itself on the formation of a stable vapor nanobubble. We determine the exact conditions under which it can be formed and compare this with the conditions that follow from a macroscopic heat balance argument. Next, we demonstrate the role of dissolved gas on the conditions required for nucleation of a nanobubble and on its growth dynamics. We find that beyond a certain threshold concentration, the dissolved gas dramatically facilitates vapor bubble nucleation due to the formation of gaseous weak spots in the surrounding liquid.

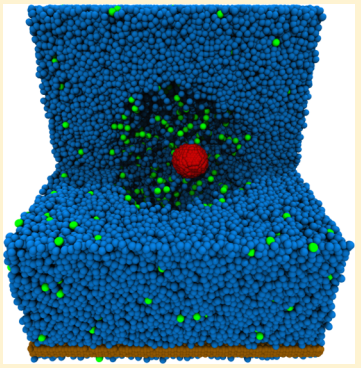

INTRODUCTION

The formation of nanobubbles around heated nanoparticles is a phenomenon that has technological relevance in applications such as cancer treatment,[1,2] catalytic reactions,[3−6] and solar energy conversion.[7,8] Nanoparticles can be heated either by exposing them to a laser pulse with a wavelength corresponding to their plasmonic resonance[1,2] or even by direct sunlight.[7,8] Exposure to high-power lasers or solar radiation raises the temperature of the nanoparticle to hundreds of kelvin,[9] leading to local heating of the liquid in their proximity to very high temperatures and eventually to the formation of a vapor nanobubble around them. These vapor nanobubbles, also known as plasmonic nanobubbles, are not only claimed to be potential candidates for efficient solar energy conversion but are also becoming a very useful tool for the therapeutic applications in cancer treatment.[1,2] In this application, the nanoparticles are engineered in such a way that they can selectively attach to the membrane of tumor cells exposing them to the high-power laser pulse and can generate nanobubbles that mechanically damage the cell membrane to destroy the tumor cells.[1,2] There have been numerous other examples where the fundamental understanding of plasmonic nanobubbles pave the way to further exploit them for a wide range of applications.[10] The formation of the nanobubble can be seen as heterogeneous nucleation where the first-order phase transition occurs at the nanoparticle present in the bulk phase. This nanoparticle facilitates the liquid−vapor phase transition. Understanding the exact mechanism of generation of plasmonic nanobubbles is also important from the fundamental point of view, since it can reveal interesting phenomena relevant to heat transfer and phase change at the nanoscale in general.[11]

The formation of a vapor nanobubble around a heated nanoparticle is a consequence of a highly out-of-equilibrium situation where the temperature gradients in the liquid can reach up to hundreds of kelvin per nanometer. The formation of a vapor nanobubble is an extremely transient process in which the bubble forms and collapses within a nanosecond. Such small time and length scales make it ideal to study the nanobubble formation by molecular dynamics (MD) simulations. Sasikumar and Keblinski[11] studied the bubble formation around a heated nanoparticle with the help of MD simulations and reported the formation of a vapor nanobubble when the temperature of the liquid in the vicinity of the nanoparticle reaches ∼90% of the critical temperature. Lombard, Biben, and co-workers[12−15] used the hydrodynamic phase field model based on free-energy density to study the threshold and kinetics of vapor bubble generation as a function of the size of nanoparticles and laser power. However, none of these studies considered the role of dissolved gas in the threshold and dynamics of nanobubble formation.

Recent experiments by Wang et al.[16] showed that dissolved gas can change the long-term growth dynamics due to diffusion of gas into the bubble. It can be argued that dissolved gas

Received: April 27, 2018
Revised: August 16, 2018
Published: August 17, 2018

DOI: 10.1021/acs.jpcc.8b04017
J. Phys. Chem. C 2018, 122, 20571−20580

should not affect the initial explosive growth which is driven by the phase change of the liquid under extreme thermal gradients, as the energy for the latent heat of vaporization is provided by the thermal diffusion, which is orders of magnitude faster than the mass diffusion of the gas in the liquid. However, dissolved gas can play a role by changing the vapor−liquid phase diagram of the system, which will influence the threshold for vapor generation. Macroscopically, it is known that homogenous nucleation of bubbles can occur at lower temperature for increased gas concentration in the liquid.[17−19] Therefore, we expect the dissolved gas not to affect the nanobubble growth dynamics but rather to affect the threshold for the formation of a vapor nanobubble around a heated nanoparticle.

To investigate the conditions for bubble nucleation and the role of dissolved gases, we perform simulations of a pure liquid around a heated nanoparticle and determine the conditions for the nucleation of a vapor nanobubble and its growth dynamics. The temperature of the nanoparticle (T_{NP}) is kept at a constant value that is much higher than the critical temperature (T_c) of the liquid. The temperature of the liquid "far away" from the nanoparticle surface is also kept constant by having an isothermal wall, the temperature of which is much lower than T_c (see Figure 1). Our results are compared to theoretical predictions based on a macroscopic heat balance.

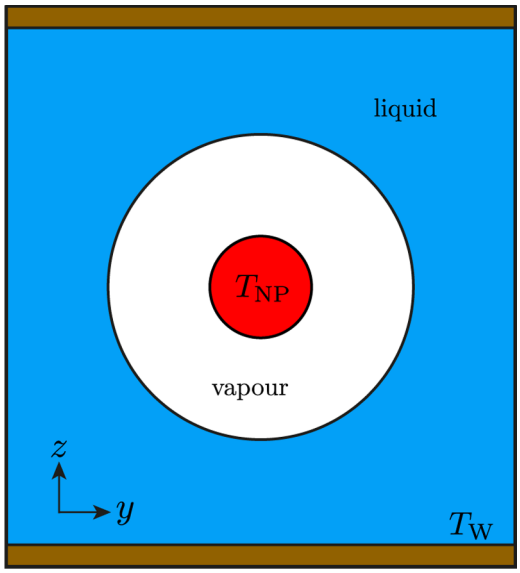

Figure 1. Schematic of a vapor nanobubble formed around a heated nanoparticle. Initially, the temperature of the whole system is constant and equal to a value T_W. At time $t = 0$, the temperature of nanoparticle T_{NP} is suddenly raised to a temperature far above T_c while keeping the wall temperature fixed at T_W.

SIMULATION METHODOLOGY

Molecular dynamics (MD) simulations were performed with the aid of the open source code GROMACS[20] to simulate the formation of a nanobubble around a heated nanoparticle. We used three types of molecules in our simulations: first acts as liquid (L), second as solid (S) and third as gas (G). The nanoparticle and wall are modeled by a collection of solid particles (S) arranged in an face-centered cubic lattice and connected with the neighboring particles by nonlinear elastic springs that act as chemical bonds. These particles can vibrate around their equilibrium positions while interacting with liquid and gas particles. They also interact with other solid particles by an interaction potential. For convenience, we refer to the type of particles that are predominantly in the liquid phase as "liquid particles" and in a similar way, we use the terms "solid particles" and "gas particles". The nonbonded interaction between the particles is described by a Lennard-Jones potential

$$V_{ij}^{LJ}(r) = 4\epsilon_{ij}\left[\left(\frac{\sigma_{ij}}{r}\right)^{12} - \left(\frac{\sigma_{ij}}{r}\right)^{6}\right] \quad (1)$$

where ϵ_{ij} is the interaction strength between particles i and j and σ_{ij} is the characteristic size of the particles. The potential is truncated at a relatively large cutoff radius (r_c) of $5\sigma_{LL}$, where σ_{LL} is the size of the liquid particles. The particles in the nanoparticle and the solid wall are connected by the finitely extensible nonlinear elastic (FENE) potential[21] as given by

$$V_{ij}^{FENE}(r) = -\frac{1}{2}k_s r_k^2 \log\left(1 - \frac{r^2}{r_k^2}\right) \quad (2)$$

where for the value of the spring constant k_s, we used $k_s = 30\epsilon_{SS}/\sigma_{SS}^2$ and for r_k, we used $1.5\sigma_{SS}$, which are consistent with the previous MD studies on nanobubble generation around a heated nanoparticle.[11,22,23] The reason for using the FENE bond potential (which is normally used for coarse-grained polymer simulations) to connect the solid particles is that this allows the nanoparticle to be heated to arbitrarily high temperatures without melting. There are around 135 000 moving LJ particles (liquid and gas) in the simulation box, whereas the nanoparticle consists of around 1400 LJ particles and the wall consists of 50 000 LJ particles. The time step for updating the particle velocities and positions was set at $dt = 0.001\sqrt{(m/k_s)}$, where m is mass of the solid particles. The mass of all Lennard-Jones particles is set as 20 Da or atomic mass unit. The time step was chosen such that its value is sufficiently smaller than the shortest time scale in the system.[24]

We now explain the choice of the boundary conditions; see Figure 1. First, in z-direction, we put in walls of constant temperature T_W to thermally equilibrate the system, as otherwise the mean temperature would keep on increasing. The input of thermal energy of the hot nanoparticle with $T_{NP} > T_W$ must be balanced. Both lower and upper wall are kept at constant temperature T_W. The wall thickness is large enough so that the LJ particles are equilibrated and no artefacts from too thin walls arise. Next, on the choice of boundary conditions in x, y-direction ("lateral"-direction, see Figure 1: we chose periodic boundary conditions for computational efficiency). This is possible and reasonable, provided that the particles at the edge of the box are so far from the hot particle in the center that they do not feel (or at least hardly feel) any thermal or density gradient caused by the heating in the center. As seen from the (latter) Figures 3 and 4, this is indeed the case. Then, the particles leaving the box on the right-hand side and entering it on the left-hand side (or vice versa) are sufficiently equilibrated and can be seen as being "at infinite distance".

Initially, the system is equilibrated at constant temperature by coupling the whole system to a constant temperature bath, equal to T_W. At time $t = 0$, liquid and gas particles are disconnected from the temperature coupling while the wall remains connected to the temperature coupling at T_W while the temperature of the nanoparticle is set to T_{NP} by coupling it

DOI: 10.1021/acs.jpcc.8b04017
J. Phys. Chem. C 2018, 122, 20571−20580

to a separate thermostat. So the gas/liquid is free to set its "own" temperature, constrained by the fixed temperatures of the wall and the nanoparticle. Two separate velocity-rescale thermostats have been used to maintain both constant T_W and constant T_{NP} with a time constant of 1 ps. T_W is chosen in such a way that it should be less than the critical temperature of the fluid, whereas T_{NP} is varied in the range such that its minimum value is always much higher than the critical temperature of the fluid. The pressure is kept constant at $p/p_c = 0.308$ (where p_c is the critical pressure of the Lennard-Jones particles) by semi-isotropic pressure coupling, which means that the simulation box can expand or contract only in the z-direction to keep the pressure constant. Berendsen pressure coupling has been used to maintain the constant pressure with compressibility equal to 4.5×10^{-5} bars^{-1} and time constant as 1 ps. The complete set of Lennard-Jones parameters that we used in our simulations are given in Table 1. The parameters for L and G particles are

Table 1. Value of Various LJ Parameters Used in the MD Simulations

i–j	σ_{ij} (nm)	ϵ_{ij} (kJ/mol)
L–L	0.34	3.0
G–G	0.5	1.0
S–S	0.30	3.0
L–G	0.42	1.73
S–L	0.32	3.0
S–G	0.42	1.0

chosen in such a way that the critical temperature of the L particles should be much higher than the highest wall temperature used in the system and for G particles the critical temperature should be much lower than the lowest wall temperature used in our simulations. The typical system size is $20 \times 20 \times 22$ nm^3 in x-, y-, and z-direction, respectively, with the z dimension changing during the simulation to maintain constant pressure.

In Figure 2, we show a typical profile of a vapor nanobubble around a heated nanoparticle for both a single-component liquid and a liquid with dissolved gas in it. The average density field of liquid particles in radial direction around the nanoparticle was calculated as a function of time to investigate the formation of a nanobubble. A nanobubble is considered to form if the density of liquid particles in the vicinity of the nanoparticle is less than the critical density of the liquid.[15] The radius R_b of the nanobubble was obtained by fitting the relation

$$\rho(r) = \frac{\rho_L + \rho_V}{2} + \frac{\rho_L - \rho_V}{2} \tanh\left(\frac{r - R_b}{w}\right) \quad (3)$$

to the radial density profile, where ρ_L is the liquid density, ρ_V the vapor density, and w the width of the liquid–vapor interface. Figure 3 shows the typical radial density profile of

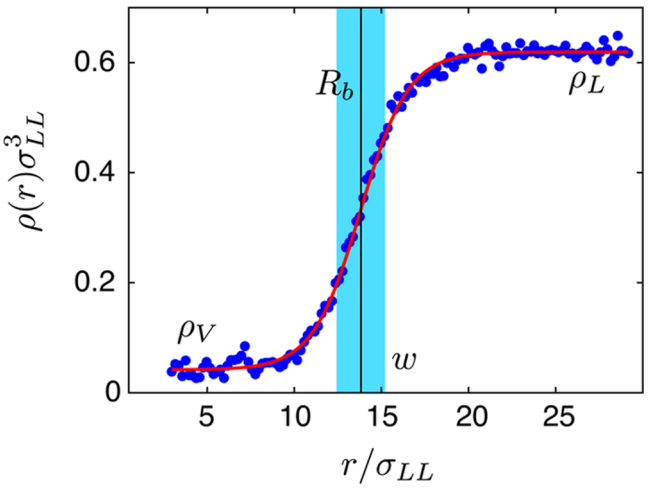

Figure 3. Radial density profile of liquid molecules around a heated nanoparticle fitted to eq 3. The black line indicates the radius of the nanobubble R_b and the shaded region depicts the width of the interface, w.

liquid particles fitted to eq 3. The density in both cases was obtained by averaging over 100 simulation snapshots with a time gap of 1000 steps between each snapshot. Note that the density of the molecules in radial direction has been calculated in two different ways: first, by assuming the center of the nanoparticle at the origin and second, by assuming the center of the nanobubble at the origin. The centers of the nanoparticle and the nanobubble are not exactly located at the same position as the nanoparticle can move a little bit inside the nanobubble. However, the position of the nanoparticle always fluctuates around the center of the nanobubble. So for better accuracy, the center of the nanobubble is used to calculate the radius while the center

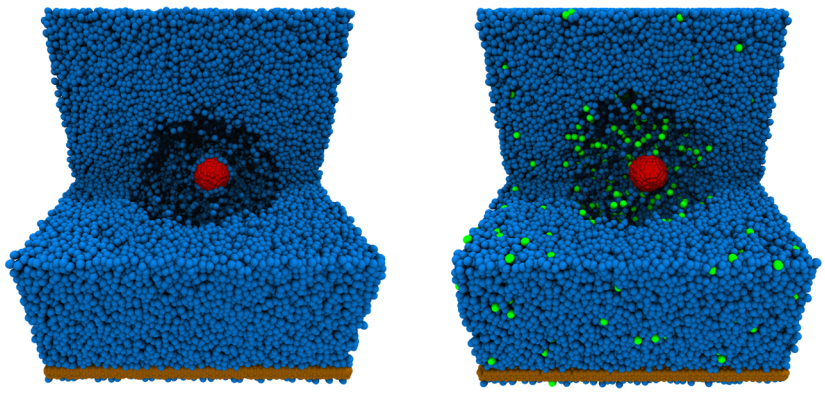

Figure 2. Typical snapshot of a vapor nanobubble formed around a heated nanoparticle for a single-component liquid (left) and with a gas dissolved in the liquid (right). In this case, $k_B T_{NP}/\epsilon_{LL}$ is equal to 5.54 and $k_B T_W/\epsilon_{LL}$ is equal to 0.97 and the mole fraction of gas molecules x_g for the snapshot on the right is set as 0.011. These snapshots are taken at 400 ps where the systems were at the steady state or "quasi equilibrium".

DOI: 10.1021/acs.jpcc.8b04017
J. Phys. Chem. C 2018, 122, 20571–20580

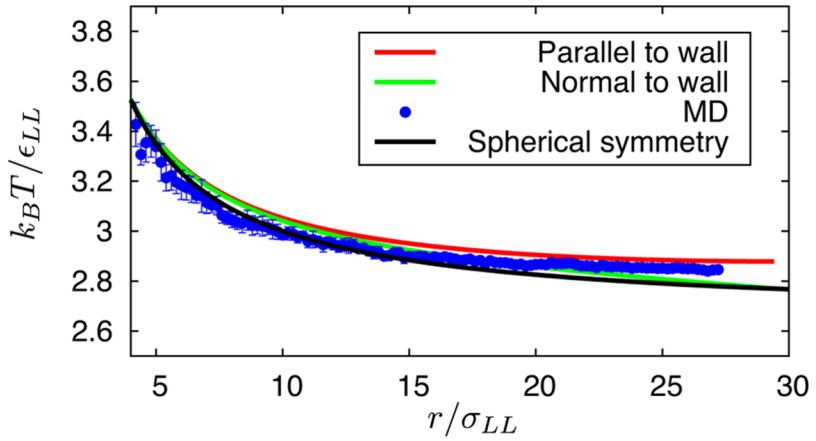

Figure 4. Temperature variation along the axis parallel and perpendicular to the wall originating from the center of the nanoparticle. The temperature profile is calculated by solving the heat equation numerically and compared with MD simulations and the spherically symmetric result. The black curve represent the analytical result obtained for perfect spherical symmetry; the red and green curves are the numerical result obtained from COMSOL for the geometry that has been used in MD simulations.

of the nanoparticle is used to calculate the density around the nanoparticle to examine the formation of the nanobubble. By "center of nanoparticle" we mean the center of mass of the nanoparticle. The center of the nanobubble is calculated by calculating the center of mass of voids present inside the nanobubble. In doing so, the whole simulation box is divided into a fine three-dimensional grid and the grid points that do not contain any LJ particle are referred to as "voids".

MACROSCOPIC MODELING

Nanobubble Formation. In this section, we describe a framework to understand the conditions that lead to the formation of a vapor nanobubble around a heated nanoparticle from a macroscopic viewpoint. As a criterion for the appearance of the nanobubble, we use the condition that the liquid temperature in the neighborhood of the nanoparticle equals the spinodal temperature T_{spin}.[1111] (A calculation of spinodal temperature T_{spin} for the single and binary mixtures of Lennard-Jones molecules is shown in the Supporting Information.)

In our MD simulations, it is shown that in the case of a vapor bubble, a layer of liquid is always formed around the nanoparticle due to high attractive force from the densely packed molecules in the nanoparticle. To be consistent with our simulations, we therefore choose the criterion that the liquid temperature at a distance $2\sigma_{LL}$ from the nanoparticle surface becomes equal to the spinodal temperature T_{spin}. We will next show that for our parameter setting, the temperature T_s' of the fluid at radius $R_p' = R_p + 2\sigma_{LL}$ is very close to the temperature T_s at the surface of the nanoparticle. Conservation of energy gives the following

$$4\pi R_p^2 G_{SL}(T_{NP} - T_s) = \frac{4\pi\kappa_L'}{R_p^{-1} - R_p'^{-1}}(T_s - T_s') \tag{4}$$

where κ_L' is the thermal conductivity of the liquid. The nanoparticle temperature T_{NP} and the liquid temperature at the nanoparticle surface T_s are related in terms of G_{SL}, the interfacial thermal conductance of the solid−liquid interface, also known as Kapitza conductance.[25] A similar statement relating the energy flow between the surface of radius R_p' and the cold wall of radius R_W at temperature T_W leads to the following

$$\frac{4\pi\kappa_L'}{R_p^{-1} - R_p'^{-1}}(T_s - T_s') = \frac{4\pi\kappa_L}{R_p'^{-1} - R_w^{-1}}(T_s' - T_W) \tag{5}$$

From the previous two equations, it follows

$$T_s - T_s' = (T_{NP} - T_W)\left[1 + \frac{\kappa_L'(R_p'^{-1} - R_w^{-1})}{\kappa_L(R_p^{-1} - R_p'^{-1})} + \frac{\kappa_L'}{R_p^2 G_{SL}(R_p^{-1} - R_p'^{-1})}\right]^{-1} \tag{6}$$

With this result we find

$$\frac{T_s - T_s'}{T_s - T_W} = \left[1 + \frac{\kappa_L'(R_p'^{-1} - R_w^{-1})}{\kappa_L(R_p^{-1} - R_p'^{-1})}\right]^{-1} \tag{7}$$

With the present parameter values, the term on the right-hand side is found to be around 0.01−0.02 so that T_s and T_s' are essentially equal.

In the previous considerations, we have assumed spherical symmetry which is clearly not fulfilled, as shown in Figure 1. Moreover the cold walls are on the top and bottom but not on the sides. To test the error associated with the spherical symmetry assumption, we numerically solved the heat conduction equation for exactly the same geometry that we used for the MD simulations, with appropriate boundary conditions, using an FEM-based commercial solver, COMSOL.[26] Figure 4 shows the temperature profile along lines originating from the center of the nanoparticle, one perpendicular to the wall along the z axis and another parallel to the wall along the y axis. The black line shows the $1/r$ behavior from the analytical solution for a spherically symmetric system. The data points in the figure show the temperature from the MD calculation averaged over spherical shells concentric with the nanoparticle. The scatter close to the nanoparticle is due to statistical fluctuations, as indicated by the error bars. There are some obvious differences between the various results, yet small enough to justify the use of the spherical symmetry assumption.

A second assumption implicit in eq 4 is that the thermal conductivity of the liquid κ_L does not vary with radial position, despite the large temperature gradient of hundreds of kelvin

DOI: 10.1021/acs.jpcc.8b04017
J. Phys. Chem. C 2018, 122, 20571−20580

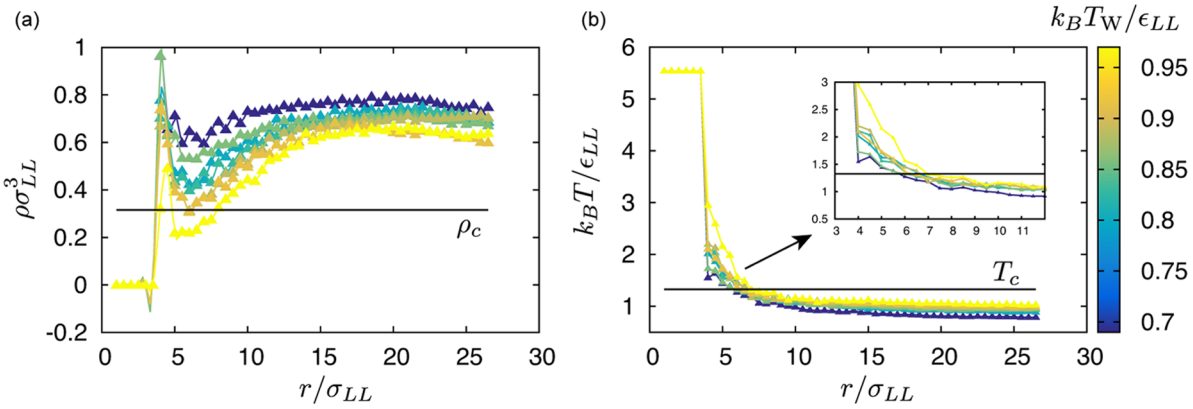

Figure 5. Variation of (a) density and (b) temperature as a function of radial distance from the center of the nanoparticle for various wall temperatures T_W. The black line indicates the critical density and critical temperature of the liquid molecules. In this case, the temperature of the nanoparticle k_BT_{NP}/ϵ_{LL} is kept at a constant value of 5.54 and the concentration of gas molecules is 0.

over a few nanometers distance. This assumption looks quite radical at the first glance due to the well-known dependence of the thermal conductivity of the Lennard-Jones liquid on the temperature and density.[27] A systematic validation of this assumption is shown in the Supporting Information.

Prediction of Maximum Bubble Radius. When a vapor nanobubble is formed around the heated nanoparticle, it grows for a while and reaches a steady state due to the finite size of the system. We can predict the steady-state radius again from the heat balance by assuming that at the liquid−vapor boundary, the temperature equals T_{spin}. At steady state, the heat coming out of the nanoparticle will get transferred across the vapor layer and exactly the same amount will be conducted through the liquid toward the cold wall. This heat balance can be written as

$$4\pi R_p^2 q = 4\pi\kappa_L \frac{1}{R_{SS}^{-1} - R_w^{-1}}(T_{spin} - T_W) \tag{8}$$

where R_{SS} is the steady-state radius of the nanobubble and q, the heat flux through the vapor phase, consists of two contributions: a conductive heat flux and a ballistic heat flux. The conductive heat flux q_c is dominated by the solid-vapor conductance $q_c = G_{SV}(T_{NP} - T_s)$, where G_{SV} is the solid-vapor interfacial conductance and T_s is the temperature of the vapor near the nanoparticle surface. The expression for the ballistic heat flux q_b for a "Knudsen gas" is given by[14]

$$q_b = \alpha\rho_s\sqrt{\frac{2k_B^3}{m}}(T_{NP}^{3/2} - T_{spin}^{3/2}) \tag{9}$$

where α is the thermal accommodation coefficient, ρ_s is the density of the liquid on the surface of the nanoparticle, and m is the mass of one liquid particle. Expression 9 for the ballistic heat flux is the difference between the energy fluxes associated with the incoming and outgoing molecules from the nanoparticle surface. The thermal accommodation coefficient α is a dimensionless parameter that characterizes the probability with which the molecules stick or leave the nanoparticle surface. From our simulations, α is calculated as follows[28,29]

$$\alpha = \frac{T_r - T_i}{T_{NP} - T_i} \tag{10}$$

where T_r and T_i are the temperatures of incident and reflected vapor molecules, respectively. The conductive flux in the vapor phase q_c is found to be at least an order of magnitude less than q_b, which is primarily due to the value of G_{SV}, which is typically 20 times smaller than G_{SL}.[14] Neglecting the contribution from q_c, we can write eq 8 as

$$\alpha\rho_s\sqrt{\frac{2k_B^3}{m}}(T_{NP}^{3/2} - T_{spin}^{3/2})R_p^2 = \kappa_L\frac{1}{R_{SS}^{-1} - R_w^{-1}}(T_{spin} - T_W) \tag{11}$$

Note that in this expression, we have assumed radial symmetry in the temperature profile of the liquid, which is less justified here as the radius of the nanobubble is comparable to the distance between the liquid−vapor interface and the wall. Nevertheless, we still used eq 11 to get a rough estimate of the maximum nanobubble radius and replaced the wall temperature T_W with the temperature averaged over a sphere of radius T_W, which is at most 10% larger than T_W. Eq 11 is solved using R_{SS} for appropriate values for the parameters and compared with the R_{SS}, as obtained from MD simulations.

RESULTS AND DISCUSSION

Formation of a Nanobubble. Figure 5 shows steady-state profiles of the liquid density and temperature around the nanoparticle obtained from MD simulations, all averaged over spherical shells. In this figure, $r = 0$ corresponds to the center of the nanoparticle, the surface of which is at $r/\sigma_{LL} \sim 5$. The various lines correspond to different cold wall temperatures for a fixed nanoparticle temperature. The horizontal black lines indicate the critical density and critical temperature of the liquid. Note that initially, the liquid around the nanoparticle has uniform temperature and density while the temperature is equal to the wall temperature T_W and the density varies according to T_W. For example, when $k_BT_W/\epsilon_{LL} = 0.69$, the initial density of the liquid is 0.78 and when $k_BT_W/\epsilon_{LL} = 0.97$, the liquid density is 0.62. The large density values at the nanoparticle surface are due to the strong attraction that the very closely spaced nanoparticle molecules exert on the liquid molecules. We consider a nanobubble to have formed when the density of the liquid molecules falls below the critical density. In the case of Figure 5a, a nanobubble is considered to have formed for the conditions corresponding to the lowest line $k_BT_W/\epsilon_{LL} = 0.97$. In this example, the minimum density is found at a distance of about $2\sigma_{LL}$ from the particle surface, a behavior that we have encountered in all examples we have studied. This is the reason why, in the macroscopic model, to

DOI: 10.1021/acs.jpcc.8b04017
J. Phys. Chem. C 2018, 122, 20571−20580

test bubble formation, we look at the temperature at a distance of $2\sigma_{LL}$ from the nanoparticle surface. Analysis of the sensitivity of the results to this particular choice is presented in the Supporting Information. The sharp drop in temperature at the nanoparticle surface visible in Figure 5b is the effect of the Kapitza resistance.

As explained before, in this work, we use two different criteria for nanobubble formation for the MD simulation and macroscopic theory. In the former one, the criterion is that the liquid density falls below the critical density of the Lennard-Jones molecules. For the macroscopic theory prediction, we use the criterion that the temperature near the nanoparticle surface exceeds spinodal temperature T_{spin}. Consistency of the two criteria requires that at the liquid−vapor interface, the density of liquid molecules should fall below the critical density and the temperature in the interfacial region should cross spinodal temperature. We tested this consistency from the measurement of density and temperature around nanoparticle when a nanobubble has been judged to form. Some typical results are shown in Figure 6 where it can be observed that critical density and spinodal temperature coincide at the liquid−vapor interface.

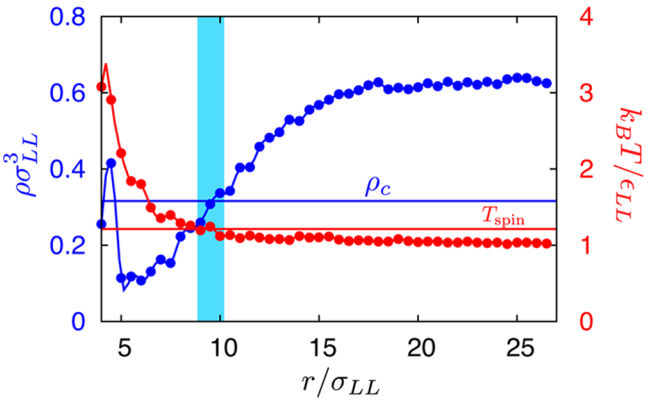

Figure 6. Variation of density and temperature around a heated nanoparticle as a function of the radial distance from the nanoparticle center. In this case, k_BT_{NP}/ϵ_{LL} is set to 5.54 and k_BT_W/ϵ_{LL} to 0.97. The shaded region indicates the liquid−vapor interface where the temperature crosses the spinodal temperature and the density of the liquid molecules goes past the critical density. It shows that both criteria for nanobubble nucleation ($T = T_{spin}$ and $\rho = \rho_c$ at the liquid−vapor interface) are consistent.

We performed simulations for various combinations of T_{NP} and T_W and identified the region in this parameter space for which a nanobubble nucleates. The results corresponding to three different gas mole fractions x_g are shown in Figure 7. Simulations were performed for three different values of the gas fraction x_g, 0, 0.011, and 0.022. The background color in Figure 7 indicates the prediction of nanobubble formation (brown = no bubble, blue = stable bubble), as obtained from the approximation $T_s \approx T_s'$ together with eqs 4 and 5

$$4\pi R_p^2 G_{SL}(T_{NP} - T_s) = \frac{4\pi\kappa_L}{R_p'^{-1} - R_w^{-1}}(T_s - T_W) \tag{12}$$

The boundary between the two colors is set by the criterion $T_s = T_{spin}$. The small circles in Figure 7 correspond to the MD simulations; colors blue and red indicate the formation or absence of a nanobubble, respectively. As expected, the results show that the nucleation of a nanobubble is more likely for

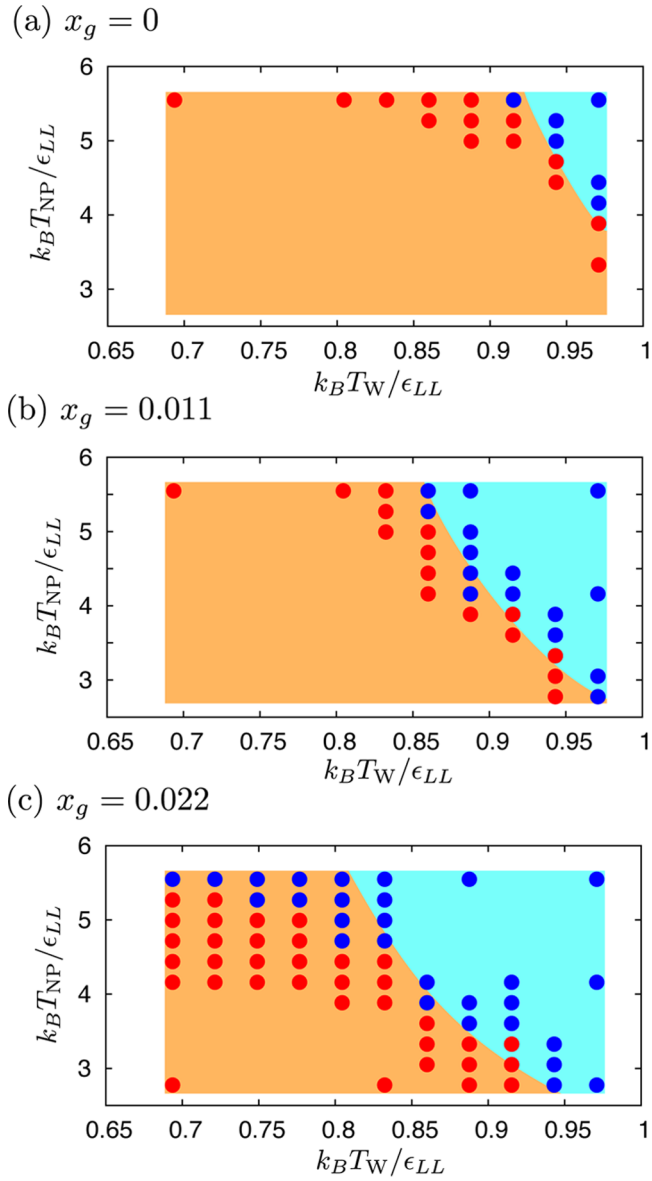

Figure 7. Values of wall temperature T_W and nanoparticle temperature T_{NP} for which a vapor nanobubble is nucleating around a heated nanoparticle when (a) $x_g = 0$, (b) $x_g = 0.011$, and (c) $x_g = 0.022$.

higher wall and nanoparticle temperatures. Figure 7a,b shows a reasonable agreement between the macroscopic theory predictions and MD simulations. However, there are clear deviations for $x_g = 0.022$ (Figure 7c), on which we will comment later.

It can be observed from Figure 7a−c that the minimum values of T_{NP} and T_W required to nucleate a nanobubble decrease significantly with an increase in gas concentration. The primary reason for this reduction is the reduction in the critical point of the binary mixture of Lennard-Jones particles. A binary mixture of Lennard-Jones particles can be approximately described as a one-component fluid with an effective interaction parameter ϵ_M. Application of the van der Waals one-fluid conformal solution mixing rules gives[30]

$$\epsilon_M = \frac{\sum_{i=1}^{n}\sum_{j=1}^{n} x_i x_j \epsilon_{ij}\sigma_{ij}^3}{\sum_{i=1}^{n}\sum_{j=1}^{n} x_i x_j \sigma_{ij}^3} \tag{13}$$

DOI: 10.1021/acs.jpcc.8b04017
J. Phys. Chem. C 2018, 122, 20571−20580

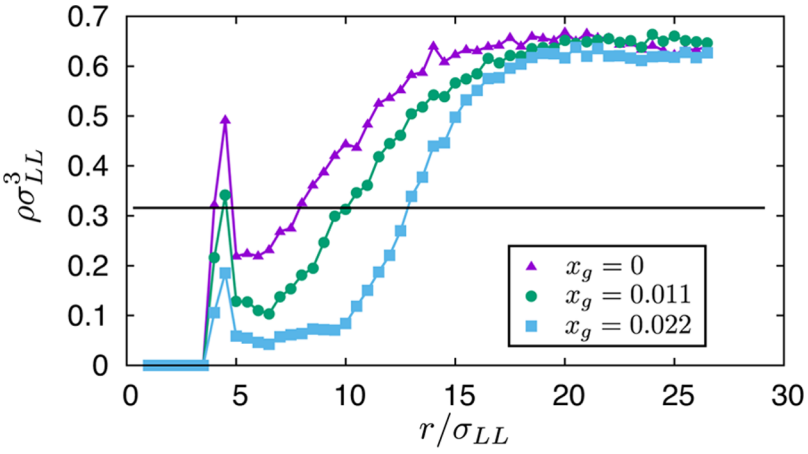

Figure 8. Density of liquid around a heated nanoparticle for various values of the mole fraction of gas molecules dissolved in liquid. T_{NP} = 2000 K and T_W = 350 K for this figure.

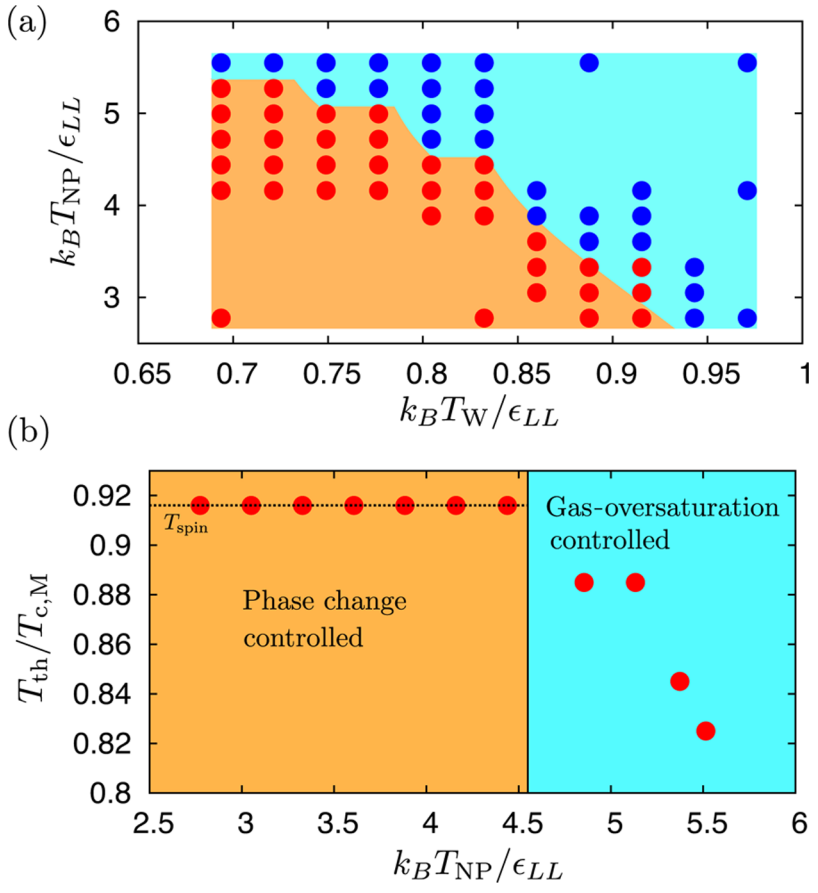

Figure 9. (a) Fitting of eq 4 with MD data of nucleation conditions for x_g = 0.022 by considering T_{th} as a fitting parameter. (b) Values of T_{th} obtained from the fit as a function of T_{NP}, which can explain the nucleation of a vapor nanobubble for x_g = 0.022. $T_{th} = T_{spin}$ shows the regime where nanobubble nucleation is controlled by latent heat required to change the phase of the mixture. $T_{th} < T_{spin}$ indicates that the nucleation of a nanobubble is controlled by the oversaturation of gas. T_{NP} at which this transition occurs should decrease with increasing x_g.

where x_i is the molar fraction of component i. In the present case, n = 2 and i = 1, 2 and ϵ_{ij} and σ_{ij} are the Lennard-Jones parameters of the mixture components. Critical temperature of the mixture is given by $T_{c,M} = 1.313\epsilon_M/k_B$.[30] For the Lennard-Jones parameters used in this study (see Table 1), the critical temperature of the single-component liquid is 474 K and that for the binary mixture of Lennard-Jones particles is 466 and 458 K when x_g = 0.011 and 0.022, respectively. There have been some experimental studies on the homogenous nucleation of bubbles in the presence of a noncondensable gas that showed similar behavior, i.e., the increase in the gas concentration decreases the saturation temperature of the liquid, which results in the nucleation of bubbles at lower temperatures compared with the pure liquid.[17,19] Although the change in the critical temperature of the mixture due to the presence of dissolved gas is relatively small, it has significant effect on the nucleation conditions, as can be observed from the shift in the boundary of nucleation boundaries in Figure 7.

DOI: 10.1021/acs.jpcc.8b04017
J. Phys. Chem. C 2018, 122, 20571−20580

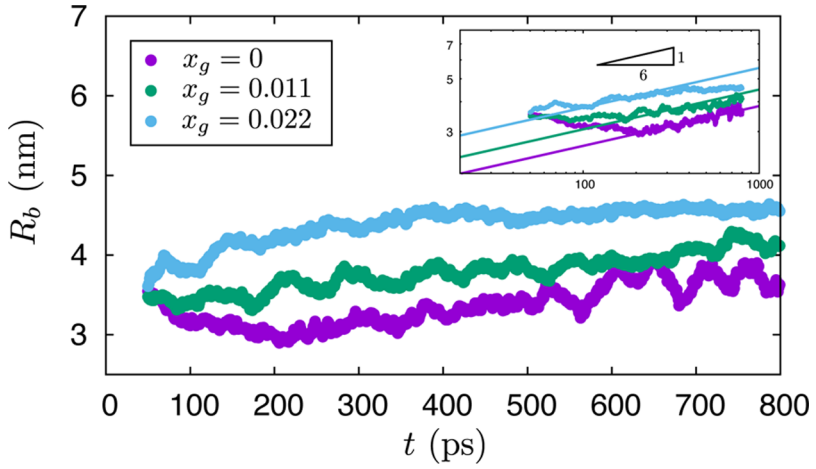

Figure 10. Radius of nanobubble as a function of time for different concentrations of gas molecules in liquid. The inset shows the same data on a log−log scale, which demonstrates that the radius of nanobubble is consistent with that for a $t^{1/6}$ behavior.

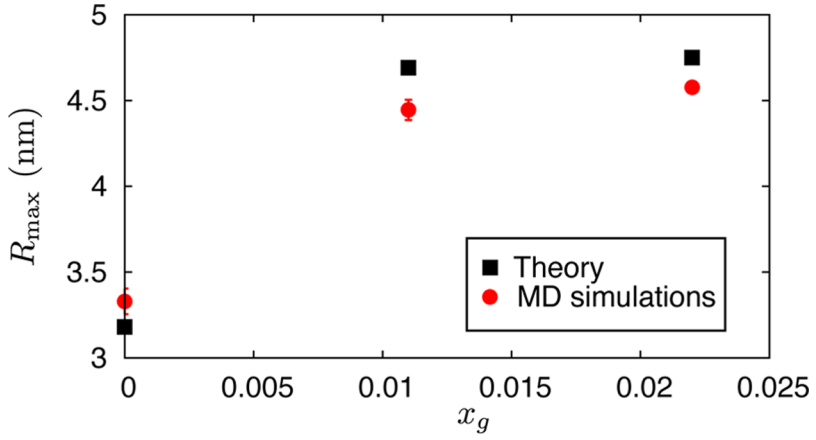

Figure 11. Steady-state radius of the nanobubble as a function of the gas mole fraction in the liquid. k_BT_{NP}/ϵ_{LL} is equal to 5.54, and k_BT_W/ϵ_{LL} is equal to 0.97 for all data points. Black data points are calculated from eq 11, which seems to be consistent with the data points obtained from MD simulations.

Figure 8 shows the density profile of liquid molecules around a heated nanoparticle for different gas concentrations at the steady state. The density near the nanoparticle decreases with increase in the gas concentration, which further demonstrates that the dissolved gas enhances the nucleation of nanobubbles.

Figure 7 clearly demonstrates that the gas molecules dissolved in the bulk liquid enhance the formation of a vapor nanobubble. However, for high gas concentration, the enhancement is more than that predicted by theory (see Figure 7c). At the highest gas mole fraction, eq 12 is clearly not able to predict the nucleation of a nanobubble at high T_{NP} and low T_W because the gas solubility decreases with increase in temperature.[31] As a consequence, the solution becomes oversaturated in the high-temperature region, which facilitates the nucleation of a nanobubble. The criterion $T_s = T_{spin}$ used before therefore fails. We can determine the appropriate threshold value $T_s = T_{th}$ from eq 4 in conditions for which the MD simulations prove the nucleation of a bubble. That is, we fit eq 4 to the boundary, as set by the MD data points of Figure 7c to obtain the values of T_{th} as a function of T_{NP}. Figure 9a shows the result of the fit, which now by construction fulfills the nanobubble nucleation conditions for $x_g = 0.022$, whereas Figure 9b shows the T_{th} normalized by the mixture critical temperature $T_{c,M}$ as a function of T_{NP} obtained from the fit. For $k_BT_{NP}/\epsilon_{LL} < 4.5$, the value of T_{th} is constant and equal to T_{spin}, suggesting that the nucleation of the vapor nanobubble can be explained by the change of phase due to the crossing of spinodal temperature near the nanoparticle surface. Beyond $k_BT_{NP}/\epsilon_{LL} = 4.5$, T_{th} decreases monotonically, which shows that the nanobubble nucleation is dictated by the high oversaturation of gas molecules near the hot nanoparticle.

Growth Dynamics. By calculating the density as a function of time after nucleation, we can follow the bubble growth. At every instant of time, we use the fit of eq 3 to determine the bubble radius. The results are shown in Figure 10. The bubble growth follows the $t^{1/6}$ behavior observed in the experiments by Wang et al.[16] This time dependence can be explained by the balancing of plasmonic heating with the latent heat of vaporization of the liquid.[16] Wang et al.[16] argued that the efficiency of heat transfer from the nanoparticle surface during the initial growth of the nanobubble is dependent on its volume. The efficiency of the heat transfer is directly proportional to the ratio of the volume of the nanoparticle to the volume of the nanobubble, which leads to the $R_b(t) \propto t^{1/6}$ behavior.[16] Although the growth dynamics of the nanobubble follows $t^{1/6}$ behavior independent of the gas concentration, the prefactor increases with the gas concentration. It can also be observed that after an initial explosive

DOI: 10.1021/acs.jpcc.8b04017
J. Phys. Chem. C 2018, 122, 20571−20580

growth, the radius of the nanobubble reaches a steady value that is due to the finite size of the system. The steady radius of the nanobubble is calculated by using eq 11 and compared with MD results in Figure 11. Note that the thermal accommodation coefficient α and the density of molecules at the nanoparticle surface ρ_s, which are input parameters to eq 11 are calculated from the MD simulation at every x_g. So in a way, the comparison of the maximum radius in Figure 11 serves as a nice consistency check between the MD simulations and macroscopic theory.

SUMMARY

Molecular dynamics (MD) simulations were performed to study the formation and growth dynamics of a nanobubble around a heated nanoparticle. The system consists of a nanoparticle dispersed in the bulk liquid that is in contact with an isothermal wall far away from the nanoparticle surface. Combinations of the nanoparticle temperature and the wall temperature that lead to the formation of a nanobubble were determined from MD simulations and were found to be in good agreement with theoretical predictions based on heat balance argument. The role of dissolved gas in the bulk liquid on the formation of nanobubble was analyzed. We found that dissolved gas enhances the nucleation of a nanobubble because of the decrease in the critical temperature of the mixture. As long as the conditions are such that the gas solution is not supersaturated, the lowering of the critical temperature is sufficient to explain the nucleation conditions. For a given gas concentration, depending on the nanoparticle and cold wall temperature, conditions can be reach to cause gas solution to become locally supersaturated. When this happens, the gas oversaturation dictates the nucleation rather than critical temperature. It would be interesting to predict this transition theoretically.

The time dependence of the radius of the nanobubble is calculated and found to follow $t^{1/6}$ behavior, in agreement with the experimental observations.[16] After the initial explosive growth, the size of the nanobubble reaches a steady state due to the finite size of the system. The steady-state radius of the nanobubble was also calculated from the heat balance arguments and was found to be consistent with the MD simulations.

ASSOCIATED CONTENT

Supporting Information

The Supporting Information is available free of charge on the ACS Publications website at DOI: 10.1021/acs.jpcc.8b04017.

Description of calculation of spinodal temperature of Lennard-Jones fluid, validity of the assumption of constant thermal conductivity made during macroscopic modeling to show the sensitivity of nucleation conditions to thickness of the liquid layer around the heated nanoparticle; details of calculation of interfacial thermal conductance and thermal conductivity of Lennard-Jones fluid used in macroscopic modeling (PDF)

AUTHOR INFORMATION

Corresponding Author

*E-mail: d.lohse@utwente.nl.

ORCID

Shantanu Maheshwari: 0000-0002-2764-6894

Detlef Lohse: 0000-0003-4138-2255

Notes

The authors declare no competing financial interest.

ACKNOWLEDGMENTS

This work was carried out on the national e-infrastructure of SURFsara, a subsidiary of SURF cooperation, the collaborative ICT organization for Dutch education and research. We thank FOM-Shell collaborative grant and MCEC for financial support.

REFERENCES

(1) Lukianova-Hleb, E. Y.; Hanna, E. Y.; Hafner, J. H.; Lapotko, D. O. Tunable Plasmonic Nanobubbles for Cell Theranostics. *Nanotechnology* **2010**, *21*, No. 085102.

(2) Shao, J.; Xuan, M.; Dai, L.; Si, T.; Li, J.; He, Q. Near-Infrared-Activated Nanocalorifiers in Microcapsules: Vapor Bubble Generation for In Vivo Enhanced Cancer Therapy. *Angew. Chem., Int. Ed.* **2015**, *54*, 12782−12787.

(3) Adleman, J. R.; Boyd, D. A.; Goodwin, D. G.; Psaltis, D. Heterogenous Catalysis Mediated by Plasmon Heating. *Nano Lett.* **2009**, *9*, 4417−4423.

(4) Christopher, P.; Xin, H.; Linic, S. Visible-Light-Enhanced Catalytic Oxidation Reactions on Plasmonic Silver Nanostructures. *Nat. Chem.* **2011**, *3*, 467−472.

(5) Baffou, G.; Quidant, R. Nanoplasmonics for Chemistry. *Chem. Soc. Rev.* **2014**, *43*, 3898−3907.

(6) Yang, J.; Li, Y.; Zu, L.; Tong, L.; Liu, G.; Qin, Y.; Shi, D. Light-Concentrating Plasmonic Au Superstructures with Significantly Visible-Light-Enhanced Catalytic Performance. *ACS Appl. Mater. Interfaces* **2015**, *7*, 8200−8208.

(7) Neumann, O.; Urban, A. S.; Day, J.; Lal, S.; Nordlander, P.; Halas, N. J. Solar Vapor Generation Enabled by Nanoparticles. *ACS Nano* **2013**, *7*, 42−49.

(8) Polman, A. Solar Steam Nanobubbles. *ACS Nano* **2013**, *7*, 15−18.

(9) Hashimoto, S.; Werner, D.; Uwada, T. Studies on the Interaction of Pulsed Lasers with Plasmonic Gold Nanoparticles toward Light Manipulation, Heat Management, and Nanofabrication. *J. Photochem. Photobiol., C* **2012**, *13*, 28−54.

(10) Lohse, D.; Zhang, X. Surface Nanobubble and Surface Nanodroplets. *Rev. Mod. Phys.* **2015**, *87*, 981−1035.

(11) Sasikumar, K.; Keblinski, P. Molecular Dynamics Investigation of Nanoscale Cavitation Dynamics. *J. Chem. Phys.* **2014**, *141*, No. 234508.

(12) Lombard, J.; Biben, T.; Merabia, S. Kinetics of Nanobubble Generation Around Overheated Nanoparticles. *Phys. Rev. Lett.* **2014**, *112*, No. 105701.

(13) Lombard, J.; Biben, T.; Merabia, S. Nanobubbles Around Plasmonic Nanoparticles: Thermodynamic Analysis. *Phys. Rev. E* **2015**, *91*, No. 043007.

(14) Lombard, J.; Biben, T.; Merabia, S. Ballistic Heat Transport in Laser Generated Nano-Bubbles. *Nanoscale* **2016**, *8*, 14870−14876.

(15) Lombard, J.; Biben, T.; Merabia, S. Threshold for Vapor Nanobubble Generation Around Plasmonic Nanoparticles. *J. Phys. Chem. C* **2017**, *121*, 15402−15415.

(16) Wang, Y.; Zaytsev, M. E.; The, H. L.; Eijkel, J. C. T.; Zandvliet, H. J. W.; Zhang, X.; Lohse, D. Vapor and Gas-Bubble Growth Dynamics around Laser-Irradiated, Water-Immersed Plasmonic Nanoparticles. *ACS Nano* **2017**, *11*, 2045−2051.

(17) Mori, Y.; Hijikata, K.; Nagatani, T. Effect of Dissolved Gas on Bubble Nucleation. *Int. J. Heat Mass Transfer* **1976**, *19*, 1153−1159.

(18) Ward, C. A.; Balakrishnan, A.; Hooper, F. D. On the Thermodynamics of Nucleation in Weak Gas-Liquid Solutions. *J. Basic Eng.* **1970**, 695.

DOI: 10.1021/acs.jpcc.8b04017
J. Phys. Chem. C 2018, 122, 20571−20580

(19) Forest, T. W.; Ward, C. A. Effect of a Dissolved Gas on the Homogeneous Nucleation Pressure of a Liquid. *J. Chem. Phys.* **1977**, *66*, 2322−2330.
(20) Hess, B.; Kutzner, C.; van der Spoel, D.; Lindahl, E. GROMACS 4: Algorithms for Highly Efficient, Load-Balanced, and Scalable Molecular Simulation. *J. Chem. Theory Comput.* **2008**, *4*, 435−447.
(21) Warner, H. R., Jr. Kinetic Theory and Rheology of Dilute Suspensions of Finitely Extendible Dumbbells. *Ind. Eng. Chem. Fundam.* **1972**, *11*, 379−387.
(22) Merabia, S.; Keblinski, P.; Joly, L.; Lewis, L. J.; Barrat, J. L. Critical Heat Flux Around Strongly Heated Nanoparticles. *Phys. Rev. E* **2009**, *79*, No. 021404.
(23) Sasikumar, K.; Liang, Z.; Cahill, D. G.; Keblinski, P. Curvature Induced Phase Stability of an Intensely Heated Liquid. *J. Chem. Phys.* **2014**, *140*, No. 234506.
(24) Frenkel, D.; Smit, B. *Understanding Molecular Simulation*; Academic Press: London, 2002.
(25) Barrat, J. L.; Chiaruttini, F. Kapitza Resistance at the Liquid-Solid Interface. *Mol. Phys.* **2003**, *101*, 1605−1610.
(26) *COMSOL Multiphysics*, version 5.2; COMSOL AB: Stockholm, Sweden, 2015.
(27) Bugel, M.; Galliero, G. Thermal Conductivity of the Lennard-Jones Fluid: An Empirical Correlation. *Chem. Phys.* **2008**, *352*, 249−257.
(28) Liang, Z.; Evans, W.; Keblinski, P. Equilibrium and Non-equilibrium Molecular Dynamics Simulations of Thermal Conductance at Solid-Gas Interfaces. *Phys. Rev. E* **2013**, *87*, No. 022119.
(29) Saxena, S. C.; Joshi, R. K. *Thermal Accommodation and Adsorption Coefficients of Gases*; Hemisphere Publishing Corporation, 1989.
(30) Harismiadis, V. I.; Panagiotopoulos, A. Z.; Tassios, D. P. Phase Equilibria of Binary Lennard-Jones Mixtures with Cubic Equations of State. *Fluid Phase Equilib.* **1994**, *94*, 1−18.
(31) Swope, W. C.; Andersen, H. C. A Molecular Dynamics Method for Calculating the Solubility of Gases in Liquids and the Hydrophobic Hydration of Inert-Gas Atoms in Aqueous Solution. *J. Phys. Chem.* **1984**, *88*, 6548−6556.

DOI: 10.1021/acs.jpcc.8b04017
J. Phys. Chem. C 2018, 122, 20571−20580